



1 Article

2 Non-invasive nanometer resolution assessment of 3 cell-soft-hydrogel system mechanical properties by scanning 4 ion-conductance microscopy

5

6 Tatiana N. Tikhonova ^{1*}, Anastasia V. Barkovaya ¹, Yuri M. Efremov ², Vugara V. Mamed-Nabizade ³, Vasili S.
7 Kolmogorov ^{3,4}, Peter S. Timashev ^{2,4,5}, Nikolay N. Sysoev ¹, Victor V. Fadeev ¹, Petr V. Gorelkin ³, Lihi Ad-
8 ler-Abramovich ⁶, Alexander S. Erofeev ³, Evgeny A. Shirshin ^{1, 5**}

9

10

11

12

13

14

15

16

17

18

19

20

21

22

23

24

25

26

27

28

29

30

31

¹ Department of Physics, M.V. Lomonosov Moscow State University, Leninskie gory 1/2, 119991, Moscow, Russia; tikhonova@physics.msu.ru, anastasia.bark18@gmail.com, nn.sysoev@physics.msu.ru, victor.fadeev@mail.ru, eshirshin@gmail.com

² Institute for Regenerative Medicine, Sechenov University, 8-2 Trubetskaya st., 119991, Moscow, Russia; yu.efremov@gmail.com

³ National University of Science and Technology "MISIS", 4 Leninskiy prospekt, 119049, Moscow, Russia; vugara2003@yandex.ru, peter.gorelkin@gmail.com, erofeev.as@misis.ru

⁴ Department of Chemistry, M.V. Lomonosov Moscow State University, Leninskie gory 1/2, 119991, Moscow, Russia; vskolmogorov@gmail.com

⁵ World-Class Research Center "Digital biodesign and personalized healthcare", Sechenov First Moscow State Medical University 8-2, Trubetskaya st., 119991, Moscow, Russia; timashev.peter@gmail.com

⁶ Department of Oral Biology, The Goldschleger School of Dental Medicine, Faculty of Medical & Health Sciences, The Center for Nanoscience and Nanotechnology, The Center for the Physics and Chemistry of Living Systems, Tel Aviv University, Tel Aviv, 69978, Israel; lihiab@gmail.com

* Correspondence: eshirshin@gmail.com, tikhonova@physics.msu.ru; +7-495-939-12-25

Abstract: Biomimetic hydrogels have increased interest due to their considerable potential for use in various fields, such as tissue engineering, 3D cell cultivation, drug delivery. The primary challenge for applying hydrogels in tissue engineering is accurately evaluating their mechanical characteristics. In this context, we propose a method using scanning ion conductance microscopy (SICM) to determine the rigidity of living human breast cancer cells MCF-7 cells grown on a soft, self-assembled Fmoc-FF peptide hydrogel. Moreover, it is demonstrated that the map of Young's modulus distribution obtained by the SICM method allows for determining the core location. The Young's modulus for MCF-7 cells decrease with the substrate stiffening, with values of 1050 Pa, 835 Pa, and 600 Pa measured on a Petri dish, Fmoc-FF hydrogel, and Fmoc-FF/chitosan hydrogel, respectively. A comparative analysis of SICM results and data obtained by atomic force microscopy were in good agreement, allowing the use of a composite cell-substrate model (CoCS) to evaluate the 'soft substrate effect'. Using the CoCS model allowed us to conclude that the MCF-7 softening was due to the cells' mechanical properties variations due to cytoskeletal changes. This research provides immediate insights into changes in cell mechanical properties resulting from different soft scaffold substrates.

Keywords: hydrogel; scaffolds; regenerative medicine; scanning ion conductance microscopy; mechanical properties; MCF-7 breast cancer cells; cell

Citation: To be added by editorial staff during production.

Academic Editor: Firstname Lastname

Received: date

Revised: date

Accepted: date

Published: date



Copyright: © 2024 by the authors.

Submitted for possible open access publication under the terms and conditions of the Creative Commons Attribution (CC BY) license (<https://creativecommons.org/licenses/by/4.0/>).

48

49

1. Introduction

50

51

52

53

54

55

56

57

58

59

60

61

62

63

64

65

66

67

68

69

70

71

72

73

74

75

76

77

78

79

80

81

82

83

84

85

86

87

88

89

90

91

92

93

94

95

96

97

98

Over the past few years, hydrogels have emerged as promising candidates for diverse biomedical applications, including drug delivery, wound healing, and tissue engineering [1-5]. Specifically, hydrogels have been developed to serve as a cell culture platform, since they effectively mimic the extracellular matrix and provide a conducive environment for cell growth and differentiation [6-8]. Due to their high water content and tunable mechanical properties, hydrogels have found extensive applications in regenerative medicine [9]. The stiffness and flexibility of hydrogels can be adjusted to mimic various tissue types, from the soft brain tissue, with a characteristic Young's modulus of $E \sim 0.1-1$ kPa [10] and adipose tissues, $E \sim 1-2$ kPa [11], to the stiffer cardiac $E \sim 30-60$ kPa [12] and bone tissues $E \sim$ tens of MPa to GPa [13-14].

Hydrogels can be broadly categorized into synthetic and natural materials [15]. Synthetic hydrogels, engineered from polymers such as polyethylene glycol and polyamides offer the advantage of tunability, where their mechanical properties can be precisely controlled by altering the crosslinking density [15]. Additionally, various factors such as amino acids, peptides, and glycans, can be incorporated into synthetic hydrogels to improve their function. However, it has been shown that cell differentiation occurs differently on stiff synthetic hydrogels compared to a natural matrix. While providing a three-dimensional environment for cell culture, rigid synthetic scaffolds cannot activate integrins and other surface receptors. In contrast, natural hydrogels contain many binding sites for integrins and growth factors that promote proper cell differentiation [16]. Moreover, natural hydrogels derived from biological sources such as collagen [17, 18], elastin [19], and fibrin [20], offer the advantage of biocompatibility and bioactivity, often promoting better cell adhesion and proliferation.

Recently, the use of Fmoc-FF peptide-based hydrogel has gained attention in the field of regenerative medicine [9, 21-23]. This hydrogel, comprising self-assembled peptide nanofibers, presents an interesting platform for cell culturing due to its unique properties [24, 25]. The softness of the Fmoc-FF hydrogel closely mimics the mechanical properties of natural tissues, making it a promising candidate for various tissue engineering applications.

There are numerous studies utilizing substrates with various topographies [26], chemical compositions [27], scales [28], and stiffnesses [29] aimed at different tissues, cells, and cellular responses. Deciphering the mechanisms and measuring the extent of influence of each of these parameters on cell populations is a complex task, as different substrate factors can influence each other. For instance, the chemical composition of substrates directly affects their stiffness [30], which in turn influences cell spreading. Consequently, cell spreading leads to high cell survival and viability.

The mechanical properties of the cell-substrate system have been the focus of numerous studies, given their direct influence on cell behavior. Such studies may include stages like obtaining cell topography on the substrate using probe or electron microscopy, obtaining the average cell stiffness in the cell-substrate system using atomic force microscopy (AFM), rheology, etc., and investigating changes in individual cell organelles during adhesion on the substrate using confocal microscopy [31-35], etc.

In recent years, the exploration of mechanical properties of materials at the nanoscale has garnered significant attention, leading to the development and application of various techniques in addition to the traditional, well-recognized AFM method. Among these, optical tweezers, as reviewed by Magazzù et al. [36], utilize highly focused laser beams to manipulate and measure the mechanical properties of soft matter at the nanoscale. For instance, optical tweezers have been used to study changes in the characteristic elasticity of cells associated with various human diseases [37, 38]. This technique is

99 particularly advantageous for its non-invasive nature and high precision; however, it is
100 effective only for manipulating very small objects, such as microparticles and molecules,
101 which limits its application to larger samples. Additionally, the method's effectiveness
102 decreases when working with thicker or opaque samples. Methods are also being de-
103 veloped that can be used directly in clinical settings to determine tissue stiffness in pa-
104 tients with diseases such as prostate cancer [39]. One such method is magnetic resonance
105 elastography. Although this technique offers a non-invasive imaging method that
106 measures the mechanical properties of tissues, making it valuable for medical applica-
107 tions, it has lower spatial resolution compared to methods like optical tweezers or AFM,
108 which may limit its application for studying small structures.

109 Here, we aim to provide a comprehensive overview of the mechanical properties of
110 the cell-hydrogel system, with a particular focus on another prominent method - the use
111 of scanning ion conductance microscopy (SICM). This technique is a powerful tool for
112 investigating mechanical properties, offering high-resolution cell imaging and quantita-
113 tive analysis [40-42]. In this study, MCF-7 breast cancer cells were chosen as a convenient
114 and well-researched model for investigating the mechanical properties of the cell-soft
115 hydrogel system using a novel alternative method, SICM. For instance, in study [43], the
116 morphology of MCF-7 cell membranes was examined in relation to substrate stiffness,
117 specifically changes in the number of microvesicles, microvilli, and the structure of filo-
118 podia. It was hypothesized that if this convenient model could show that the SICM
119 method allows for a deep characterization of the cell-soft hydrogel system, with the sub-
120 strate stiffness being lower than that of the cells, and that the self-assembling Fmoc-FF
121 hydrogel would be a promising biocompatible scaffold for these cells, then this method
122 could be used in the future to study various epithelial/neural or other cell types. This
123 approach can examine cell-hydrogel system dynamics, allowing the evaluation of cell
124 mechanical characteristics following treatment with drugs and growth factors or hydro-
125 gel degradation. The novelty of this study lies, firstly, in obtaining a mechanical property
126 distribution map of live cells on Fmoc-FF hydrogel, which can be considered a potential
127 material for use as an extracellular matrix (ECM). Furthermore, to the best of our
128 knowledge, there are no studies dedicated to obtaining a mechanical property map in a
129 cell-substrate system where the substrate is softer than the cell.
130

131 2. Results

132 2.1. The mechanical properties of the cells-hydrogel system assessed using SICM.

133 The topography and Young's modulus distribution of low aggressive human breast
134 cancer cells MCF-7 placed on the Petri dish and self-assembled soft Fmoc-FF hydrogel are
135 presented in Fig. 1. The investigations were carried out by SICM, and the mechanical
136 properties were calculated via disjoining pressure. The topography of MCF-7 cells ex-
137 hibited a typical epithelial-like structure with cell-cell contacts in the Petri dish, with
138 various microvilli on their surface (Fig. 1A). This observation agrees with SEM investi-
139 gations [43]. The quantitative mechanical cell's mapping of cells' mechanical properties is
140 presented in (Fig. 1B), the average Young's modulus value was $E_{\text{mean}} = 1050 \pm 55$ Pa. The
141 topography of cells placed on the soft hydrogel is presented in Fig. 1C.

142 In this work, for the first time, the mechanical properties distribution for cell-soft
143 hydrogel system in an aqueous solution with nanometer resolution are presented; see
144 (Fig. 1D). In the inset of Fig. 1C the morphology of soft Fmoc-FF hydrogel can be seen
145 (see Fig. 1E)): the biomaterial is comprised by the fibers with the characteristic length
146 from several to tens micrometers and with the fiber's width ~ 150 -250 nm. This data is in
147 good agreement with confocal fluorescence microscopy (Fig. S1).
148

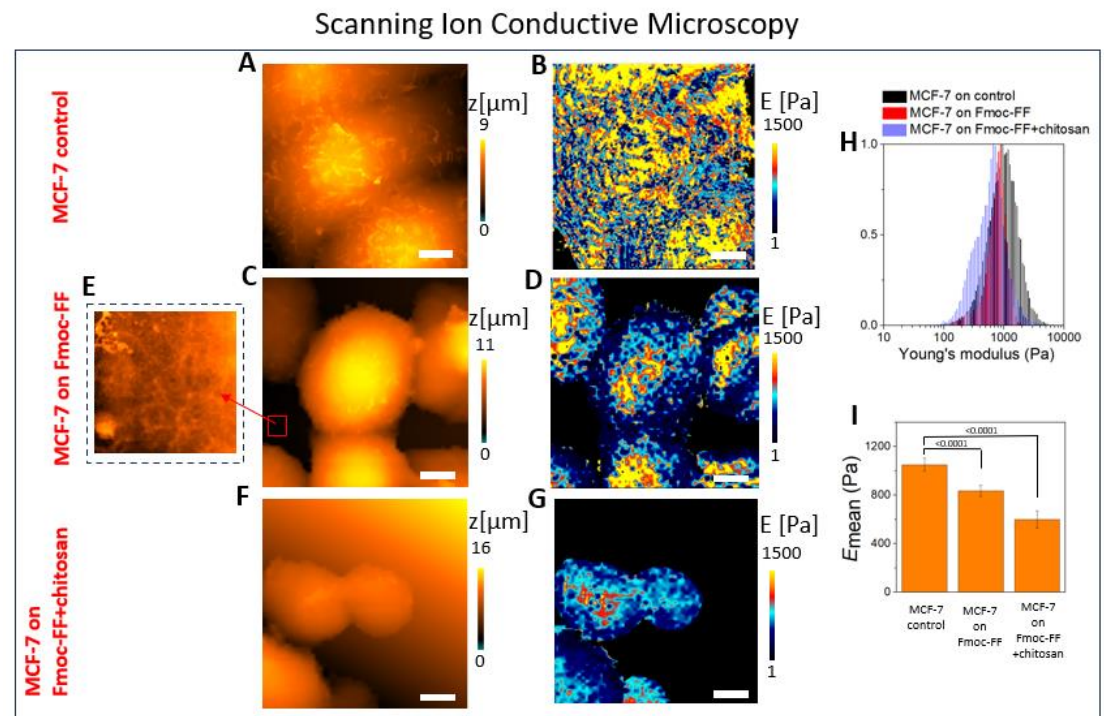


Figure 1. The SICM topography image of MCF-7 cells placed on (A) a cultural Petri dish, (C) Fmoc-FF hydrogel and (F) Fmoc-FF+chitosan hydrogel. The distribution of Young's modulus for MCF-7 cells placed on (B) cultural Petri dish, (D) Fmoc-FF hydrogel and (G) Fmoc-FF+chitosan hydrogel, $C_{\text{Fmoc-FF}}=0.6\%$, $C_{\text{Fmoc-FF}}:C_{\text{chitosan}}=10:1$. (E) The SICM topography image of Fmoc-FF hydrogel. (H) The histogram of Young's modulus distribution for MCF-7 cells placed on cultural Petri dish (control, black lines), Fmoc-FF hydrogel (red lines) and Fmoc-FF+chitosan hydrogel (violet lines). (I) The cell Young's modulus for MCF-7 on control, Fmoc-FF hydrogel, and Fmoc-FF+chitosan hydrogel systems. The scale bar is 5 μm . The radii of capillaries were $R_{\text{cap}}=45$ nm.

Comparing cell topography on a Petri dish and hydrogel (Fig. 1A) and (Fig. 1C), correspondingly, it can be seen that MCF-7 cells shape varies being spread on the stiff Petri dish, cells are characterized by rounded shape when placed on the soft hydrogel. The profiles of cells placed on Petri dish and Fmoc-FF hydrogel can be seen in Fig. S2. Moreover, the microvilli that were clearly seen on the rigid substrate (Petri dish) disappeared (or greatly diminished in number) on the soft hydrogel. It should be noted that the images (Fig. 1A and 1C) were obtained with the same resolution, using the capillaries with the $R_{\text{cap}}=45$ nm, so the observed changes were due to the cells' structure variations. Microvilli are finger-like protrusions whose shape is controlled by the actin bundles [44]. Franchi et al. demonstrated by SEM-analysis that for MCF-7 cells, the densely packed collagen fibers that served as a substrate for cells stimulated the develop many cytoplasmic microvilli in contrast with low concentrated type I collagen-covered substrate, which is in agreement with our observations.

Moreover, cells were also placed on the Fmoc-FF hydrogel, where the low molecular chitosan was added. Chitosan, being a polysaccharide extraction from natural chitin, attracts attention in the field of tissue engineering due to its ability to increase the cell viability [45-47], biocompatibility and biodegradability [48]. The SICM topography and the distribution of Young's modulus images of MCF-7 cells placed on Fmoc-FF hydrogel+chitosan can be seen on Fig. 1F and 1G, correspondingly.

More than 40 cells were processed for each sample. Fig. 1H shows the typical histogram of Young's modulus distribution for MCF-7 cells placed on cultural Petri dish

(control, black lines), Fmoc-FF hydrogel (red lines) and Fmoc-FF+chitosan hydrogel. It should be noted that the distribution that corresponds to the MCF-7 on Fmoc-FF and Fmoc-FF+chitosan hydrogel system (red and violet lines) had a bimodal character originated from two components: the MCF-7 cells and hydrogel. To clarify the bimodal nature of system the Fig. 1H was divided into three separate figures and also presented in SI, see Fig. S3.

In Fig. 1I the Cells' Young's modulus on the substrate with different stiffness is presented for MCF-7 on control, Fmoc-FF and Fmoc-FF+chitosan gels. Chitosan, incorporated into the hydrogel structure, interferes the peptide self-assembly process, leading to hydrogel's softening.

The data obtained in Section 2.1 would be used to assess the adequacy of the alternative SICM method compared to the traditional AFM method for determining the mechanical properties of the cell-soft hydrogel system. The data of AFM analysis would be performed in Section 2.3.

2.2. The correlation of MCF-7 Young's modulus distribution with fluorescence imaging

To find out if the obtained Young's modulus distribution describes the real cell's structures, the nuclei, and microtubules were stained with *Hoechst* 33258 and Tubulin-Tracker™ Green, correspondingly. Fig. 2 demonstrates the optical image, topography, Young's modulus distribution, fluorescence image of the stained nucleus, and microtubules that were obtained for one cell on control and Fmoc-FF hydrogel.

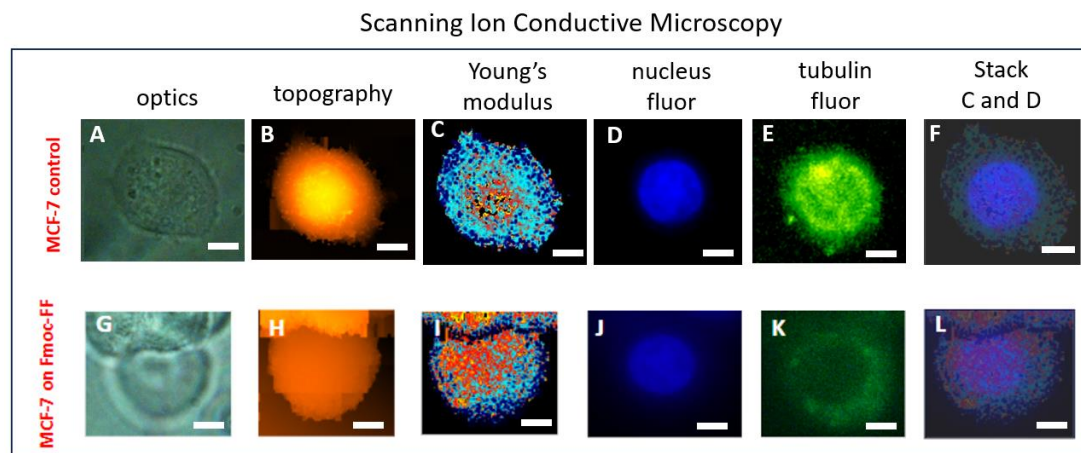


Figure 2. (A, G) optical images, (B, H) topography, (C, I) Young's modulus distribution, (D, J) fluorescence image of nuclei, (E, K) fluorescence image of tubulin, (F, L) stack images of Young's modulus distribution and fluorescence image of nuclei for MCF-7 cells placed on cultural Petri dish and Fmoc-FF hydrogel, correspondingly. The scale bar is 5 μm .

Comparison of Young's modulus distribution as for MCF-7 placed on a Petri dish (Fig. 2C) and Fmoc-FF hydrogel (Fig. 2I) with the fluorescence images of their nuclei (Fig. 2D, 2J) and tubulin (Fig. 2E, 2K) demonstrates that the stiffest regions on the Young's modulus distribution map (represented by orange and yellow colors in Fig. 2C, 2I) correspond to areas where the cell nucleus is located, whereas the softer regions (indicated by light blue and blue colors in Fig. 2C, 2I) along the cell periphery correspond to the cytoskeleton.

2.3. The mechanical properties of the cells-hydrogel system assessed using AFM

The same systems were examined using the AFM technique. In Fig. 3 the optical images (panels A, D, G), topography (panels B, E, H) and Young's modulus distribution (panels C, F, I) for MCF-7 cells on Petri dish, Fmoc-FF hydrogel and Fmoc-FF+chitosan hydrogel) are presented.

Due to high softness of the cells and the gels, and also due to large cell height, the force maps had artificial stripes along the scanning directions. The affected force curves with a low quality fit with the Hertz's model were excluded from the analysis. The typical force curves for all the samples can be seen in Fig. S4.

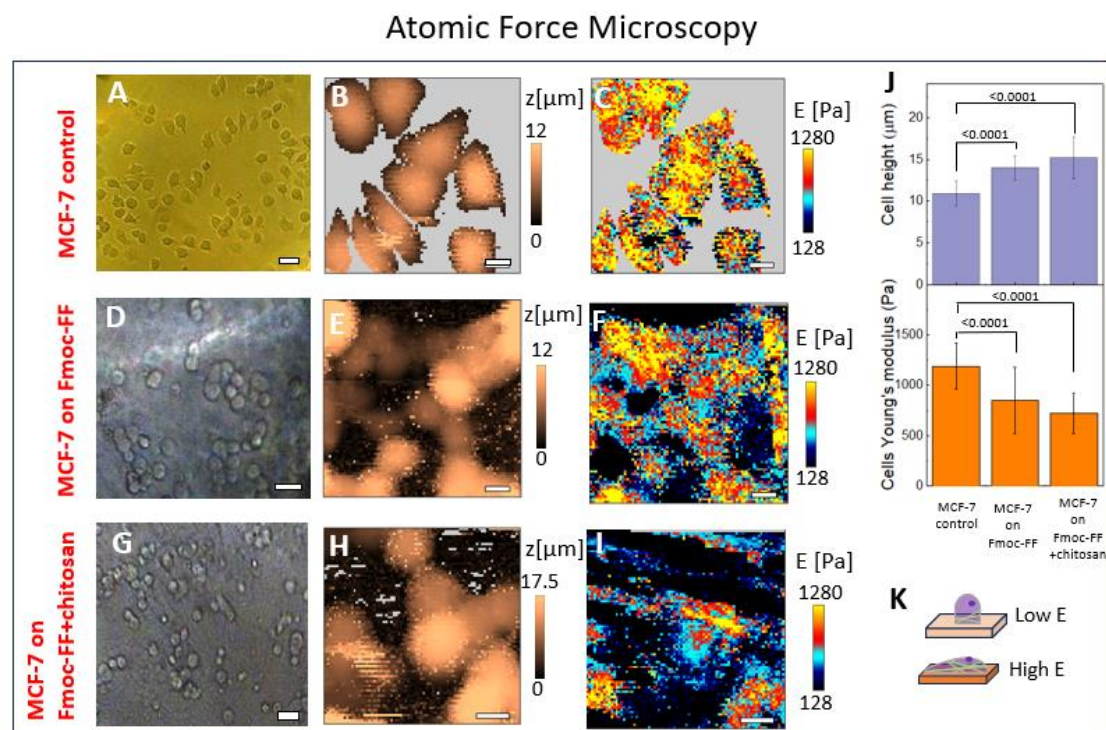


Figure 3. The optical images (A, D, G), topography (B, E, H) and Young's modulus distribution (C, F, I) for MCF-7 cells on Petri dish, Fmoc-FF hydrogel and Fmoc-FF/chitosan hydrogel, correspondingly. (J) The cell height and cell Young's modulus for MCF-7 on control, Fmoc-FF hydrogel, and Fmoc-FF+chitosan hydrogel systems. (K) The schematic images for cells placed on low and high modulus substances. The scale bar for optical images is 40 μm , the scale bar for topography, and Young's modulus images are 10 μm . $C_{\text{Fmoc-FF}}=0.6\%$, $C_{\text{Fmoc-FF}}:C_{\text{chitosan}}=10:1$. Statistical significance was probed with Kruskal-Wallis non-parametric test and Dunn's correction for multiple comparisons. $R_{\text{tip}} = 70 \text{ nm}$.

Both optical images show that the shape of the cells changes significantly depending on the substrate: being spread on the stiff Petri dish, they become more rounded on the soft hydrogels. These data are in agreement with the results obtained by the SICM method. In Fig. 3J correspondence of Cells' Young's modulus, cells' height on the substrate with different stiffness is presented for MCF-7 on control, Fmoc-FF and Fmoc-FF+chitosan gels. Chitosan, incorporated into the hydrogel structure, interferes the peptide self-assembly process, leading to hydrogel's softening (Fig. 3J). Namely, Young's modulus for the Fmoc-FF+chitosan system was $E_{\text{mean}}=450\pm140 \text{ Pa}$, whereas for the Fmoc-FF gel $E_{\text{mean}}=500\pm170 \text{ Pa}$, and the mean height of cells on Fmoc-FF+chitosan exceeded that for Fmoc-FF: $H_{\text{mean}}(\text{Fmoc+chitosan}) = 15.2\pm2.4 \mu\text{m}$ and $H_{\text{mean}}(\text{Fmoc}) = 14\pm1.5 \mu\text{m}$, correspondingly. At that, the mean height of cells on the Petri dish was $H_{\text{mean}}(\text{Petri dish}) = 10.9\pm1.5 \mu\text{m}$. These data were taken from the processing of 40 cells for each sample. The

schematic illustration of the cell's shape depending on the substrate stiffness is presented in Fig. 3K.

Comparing the Young's modulus distribution for all the investigated systems, it should be noted that the AFM data is in good agreement with SICM studies: $E_{\text{mean}} = 1190 \pm 230$ Pa for MCF-7 cells on Petri dish, $E_{\text{mean}} = 980 \pm 240$ Pa for MCF-7 cells on Fmoc-FF hydrogel, also see Table in the Discussion section. However, the SICM topography and quantitative mechanics mapping had higher resolution (see Fig. 1 and 3): for instance, in images acquired using SICM, the distribution of Young's modulus of both the cells themselves and the gel is readily discernible. In contrast, the Young's modulus for cells and gel obtained through AFM appears similar to each other and is challenging to differentiate them visually. In AFM experiments, the resolution (80x80 points) was limited to improve the data acquisition speed and to avoid the excessive sample damage due to repeated indentations. When comparing the topography obtained by both methods, it can be observed that while microvilli with an approximate width of 200-250 nm are visualized using the SICM technique (see Fig. 1A), they are not discernible in images acquired through the AFM method (see Fig. 3B). This fact can be explained as follows: the resolution depends on contact radius, the contact radius depends on indentation that, in turn, depends on sample stiffness. The resolution reduction for AFM data can be explained by higher values of applied forces and higher values of indentation in comparison with SICM technique: for example, while the mean indentation for MCF-7+Fmoc-FF hydrogel system was 1500 nm in AFM experiments, for the same sample the indentation was evaluated as 220 nm in SICM studies.

2.4. The Swelling determination of soft Fmoc-FF hydrogel

The primary research in this article focused on studying the mechanical properties of the cell-soft hydrogel system using the SICM method and comparing the obtained data with those from the traditional AFM method. In order to consider this hydrogel as potential scaffold in the regenerative medicine its biocompatibility with living cells was examined. When studying the biocompatibility of hydrogels with cells, there is a set of scaffold characteristics that can directly affect cell viability on them. These characteristics include the swelling and degradation of hydrogels. These properties are important because the hydrogel is intended to mimic the extracellular matrix, which is largely composed of water. So, we also conducted swelling studies on Fmoc-FF peptides. The swelling data for Fmoc-FF hydrogels were obtained after incubating the hydrogels in a large volume of PBS (pH 7.4) at 37°C for 24 hours. The results, expressed as the swelling ratio q . It was found that all hydrogels exhibited very high swelling ratios, with q reaching 98%. Sample weight loss measurement data showed that, the gels completely degraded within 35 days of incubation, as shown in Fig. S5.

2.5. Biocompatibility of soft hydrogels

After that the test that describes the biocompatibility of the self-assembling gel and living cells, which is a necessary experiment when proposing a hydrogel as a scaffold was carried out: MCF-7 cells were placed on the Fmoc-FF hydrogel, which was formed on confocal Petri dishes and washed for 2 days with PBS in order to remove the excess DMSO and to set the hydrogel pH to 7.3 [24]. After that the samples were UV sterilized. In two days, the live/dead test was carried out using C12 resazurin, a cell membrane dye indicating metabolically active cells (red), and DAPI, a DNA stain indicating dead cells (blue), Fig. S6A. In addition, Live/dead test demonstrated that there was a dominant population of red cells on Fmoc-FF hydrogel. However, few blue (dead) cells were also found (more than 20 images were studied, each of which contains ~50 cells).

290 Cytocompatibility was also examined for MCF-7 cells on Fmoc-FF and
291 Fmoc-FF/chitosan hydrogels (Fig. S6B). For this purpose, DMEM culture medium was
292 incubated with Fmoc-FF and Fmoc-FF+chitosan hydrogels overnight. This medium was
293 then extracted from the hydrogels and added to MCF-7 cells, whose viability was as-
294 sessed after 24 hours of incubation. It can be seen that the presence of chitosan markedly
295 increased cell survival – from 40% up to 80%.

296 *2.6. Comparison of Fmoc-FF hydrogel biocompatibility prepared by pH-switch and solvent* 297 *switch methods.*

298 Since in section 2.5 low biocompatibility of the Fmoc-FF hydrogel with cells was
299 demonstrated, the question arose whether this result is due to the method of hydrogel
300 preparation or if it is a consequence of the peptide composition of the hydrogel. The
301 self-assembled Fmoc-FF hydrogel can be prepared using two methods: by solvent switch
302 and pH switch methods. In this work, the hydrogel was prepared by the solvent switch
303 method: the peptide was dissolved in dimethyl sulfoxide (DMSO) and then diluted in
304 distilled water to a final concentration of $C_{\text{Fmoc-FF}}=0.6\%$, the final concentration of DMSO
305 in the solution was 6%. The 6% concentration of DMSO in hydrogel can reduce cell sur-
306 vival [49]. To avoid this effect, the hydrogel was washed for two days with PBS to com-
307 pletely remove excessive DMSO [22]. However, to ensure that it is not excessive DMSO
308 that affects cell survival on hydrogels, a Fmoc-FF gel was prepared using the pH switch
309 method. The gel was made according to known procedure [50]: Fmoc-FF peptide was
310 dissolved in water, $C_{\text{Fmoc-FF}}=0.6\%$, then NaOH (0.5 M) was added to the solution so that
311 the pH of the solution was adjusted to pH 9, the solution was stirred using a magnetic
312 stirrer. Thereafter glucono-delta-lactone (GdL) was added to lower the pH to 4, and then
313 the gel was formed and washed with PBS for several hours to adjust pH to 7.3 [24]. Cell
314 biocompatibility tests were performed on Fmoc-FF and Fmoc-FF+chitosan hydrogels
315 (live/dead test and MTT test) that were prepared by pH switch methods. The results
316 showed that the gel preparation method did not affect the cell survival on the hydrogel
317 (data not shown). So, we concluded that cell viability was not influenced by the potential
318 residual amount of DMSO in the case of hydrogel preparation by solvent switch method.

319 **3. Discussion**

320 The main aim of this work was to investigate the mechanical properties of living cell
321 -soft hydrogel system using SICM, that is able to provide the high resolution, $R=40\text{ nm}$,
322 in aqueous solution. For the first time, the quantitative nanomechanical distribution of
323 cells- soft hydrogel system was obtained, see Fig. 1D, which enables estimation of the
324 mechanical properties for both soft biomaterial and cells placed on it.

325 Staining of the nucleus and microtubules within cells has enabled the demonstra-
326 tion that the Young's modulus distribution map, obtained via SICM, reflects specific
327 cellular structures: namely, the nuclei (the stiffest part of the cells) and the cytoskeleton in
328 the peripheral regions of the cells, see Fig.2. The obtained data can be used to investigate
329 the more detailed response of cells to the influence of scaffolds on them.

330 In 2021, the authors Taira et al. [51] presented the topography of endothelial cells
331 placed on collagen hydrogel with nano-resolution obtained using SICM for the first time.
332 However, no quantitative mechanical nano-mapping for the cell-soft-hydrogel system
333 was presented. Also, Schierbaum, et al [52] obtained the stiffness of living fibroblasts at
334 high resolution, $R=1\ \mu\text{m}$, placed on polyacrylamide hydrogel using AFM. At that it
335 should be noted that the cell was placed on rather rigid hydrogel with the Young's
336 modulus $E=6.0\pm 0.4\text{ kPa}$, and the mechanical distribution was represented only for cell
337 structure without mapping the hydrogel Young's modulus.

Table 1. The mean Young's modulus for 3 systems: MCF-7 on Petri dish (control), MCF-7 on Fmoc-FF hydrogel, MCF-7 on Fmoc-FF/chitosan hydrogel. $C_{\text{Fmoc-FF}} = 0.6\%$, $C_{\text{Fmoc-FF}}: C_{\text{chitosan}}=1:1$. The data was obtained by SICM and AFM methods.

		SICM	AFM	AFM, CoCS model
MCF-7 on Petri dish, E, Pa		1050±55	1190±230	1190±230
MCF-7 on Fmoc-FF hydrogel, E, Pa	MCF-7	835±45	980±240	1060±250
	Fmoc-FF	300±30	500±170	500±170
MCF-7 on Fmoc-FF +chitosan hydrogel, E, Pa	MCF-7	600±70	860±220	930±230
	Fmoc-FF+chitosan	270±60	450±140	450±140

If we compare the values of Young's modulus, obtained by AFM, of cells, placed on Petri dish and different hydrogels we can see the following dependence: the mean E for cells were 1190, 980, and 860 Pa placed on the most rigid substrate (Petri dish), Fmoc-FF and Fmoc-FF/chitosan with mean E of 500 and 450 Pa. Hence, the less rigid the substrates were, the softer the cells became. The main question was if the cells' mechanical properties changed due to the cytoskeletal changes in response to their substrates' stiffness or it was the result of indentation of substrate that is softer than the cells itself.

Herein the question of substance softness effect on the mechanical measurements should be discussed. The cell on the surface of the hydrogel that is softer than the cell itself can seem softer due to an unaccounted deformation of the underlying substrate during the indentation, that is called 'soft substrate effect'. To account for this effect Rheinlaender et.al. suggested a composite cell-substrate model (CoCS) [53], where they represented the total indentation in the experiment as the sum of cell and soft substrate indentations on the example of AFM studies. In this study, a good correlation between the AFM and the SICM methods was demonstrated, as shown in Table 1. So, here, we provide an assessment of how much the cell stiffness might be underestimated in our experiments, using the CoCs model for the spherical indenter using AFM method and draw conclusions for both methods given the good agreement of the data between them

We calculated this underestimation in the cell Young's modulus obtained by AFM method taking into account the typical values of the hydrogel Young's modulus (450-550 Pa), cell Young's modulus (800-1000 Pa), radius of the probe (70 nm), applied load force (0.1-0.2 nN at 500 nm depth) and radius of a cell bound to a substrate (10 μm). The obtained estimate was ~7-8%, i.e., relatively small due to a small radius of the used AFM probe, so, this correction should be considered for the estimation of cell's stiffness on soft Fmoc-FF hydrogels. Overall, softening of the cell on hydrogel was not due to an underestimation of the stiffness of the cell on a soft substrate, but was caused by a change in its intrinsic mechanical properties.

Also, the obvious cell shape change was observed in the SICM and AFM experiments during the MCF-7 adhesion on the soft hydrogels in comparison with the stiff Petri dish. The round shape of cells placed on biomaterial versus a spread shape of MCF-7

placed on a Petri dish can be explained by the change of substrate stiffness, see Fig.3 J, K, that is in accordance with the investigation of direct influence of matrix stiffness on cells shape [54-56]. It was demonstrated that such morphology changes of cells in response to the substrate stiffness is due to the cytoskeleton variation, specifically to the dense and length of actin fibers. Hogrebe et al. demonstrated that spread cells, placed on the stiff substrate, are characterized by long actin fibers, and their amount increased with the stiffness rising [54]. Moreover, the changes in the substrate stiffness led to different proliferation and differentiation pathways for cells.

Here, it should be noted that not only the substrate's stiffness, but also different functional groups contained on Fmoc-FF hydrogels and on cultured Petri dishes could affect the shape change of MCF-7 cells, which is another factor affecting the topography of cells adsorbed on the substrate [27]. By JC Gil-Redondo, et. al. [57] it was investigated how the substrate stiffness modulated the viscoelastic properties of MCF-7 cells that were placed on polyacrylamide hydrogels. Polyacrylamide hydrogel substrates with varying Young's moduli of 0.1 kPa, 4.1 kPa, and 17.3 kPa were considered. The study demonstrated that substrate stiffness had a similar effect on MCF-7 cells as observed in our study, specifically that with increasing substrate stiffness, MCF-7 cells transitioned from a spherical shape at $E_{\text{substrate}}=0.1$ kPa to a more spread-out form at $E_{\text{substrate}}=17.3$ kPa. This effect was shown using polyacrylamide hydrogel, where the functional groups on the surface remained unchanged with varying stiffness. This could indicate that in our experiment the primary contribution to the change in the shape of MCF-7 cells was due to the alteration in substrate stiffness of Fmoc-FF hydrogels, rather than differences in the functional groups of the gels and the Petri dish.

Another factor that may influence the change in cell shape is their viability on a given substrate. Indeed, cells can change their shape due to the low viability on the Fmoc-FF gel (see Fig. S6B). However, it should be noted that cells on the Fmoc-FF+chitosan gel also exhibit a round shape, even though cell viability on the Fmoc-FF+chitosan gel is high (see Fig. S6B). In the article by JC Gil-Redondo et al. [57], the change in the shape of MCF-7 cells placed on a polyacrylamide gel, which is biocompatible and widely used in regenerative medicine [58], is considered. The study shows that the shape of MCF-7 cells is spherical when they are adsorbed on a soft polyacrylamide gel with a Young's modulus of 0.1 kPa, whereas increasing the stiffness of the substrate leads to cell spreading. From this, it can be concluded that the stiffness of the hydrogel is the primary factor affecting cell shape.

The biocompatibility analysis for MCF-7 cells on Fmoc-FF hydrogel, $C_{\text{Fmoc-FF}} = 0.6\%$, demonstrated that Fmoc-FF hydrogel is unsuitable for using this biomaterial as scaffold. However, the incorporation of chitosan into Fmoc-FF hydrogel, that is known due to its ability to increase biocompatibility and biodegradability [45-48] increase the cells viability from 40% up to 80%. It was demonstrated that the method of hydrogel preparation (solvent switch and pH switch) does not affect cell viability, so low value of biocompatibility was addressed to the chemical structure of hydrogel.

4. Materials and Methods

4.1. Sample preparation

(A) Reagents. The N-fluorenylmethoxycarbonyl diphenylalanine peptide (Fmoc-Phe-Phe-OH, Fmoc-FF), chitosan ($M = 190$ kDa), *Hoechst* 33258 were purchased from Sigma-Aldrich (USA), N-Fmoc-2,3,4,5,6-Pentafluoro-L-phenylalanine (Fmoc-Phe(F5)-OH, Fmoc-F5) was purchased from GL Biochem (Shanghai, China), Dulbecco's Modified Eagle's Medium (DMEM) was purchased from Gibco (USA), Tubulin-Tracker™ Green was purchased from Thermo Fisher Scientific (USA).

(B) Hydrogels. The Fmoc-FF hydrogel was prepared using two methods: a) the solvent-switch method and b) pH-switch method. The hydrogels using solvent-switch method were prepared as follows: the peptides were dissolved in dimethyl sulfoxide (DMSO) to obtain the stock solution, $C_{\text{Fmoc-FF (stock)}} = 10\%$, then the stock solution was dissolved in milli-Q water to a final concentration of $C_{\text{Fmoc-FF}} = 0.6\%$ [21, 59]. The preparation of hydrogels using the pH-switch method was performed as follows: the weighted peptides were added to milli-Q water, and after that, NaOH solution (0.5 M) was added. The solution was vortexed and sonicated to facilitate mixing until the solution became transparent. The gelation process was initiated by incorporating glucono-d-lactone (GdL) into the basic peptide solution and mixing was accomplished by vortexing for a duration of 5 seconds. The sample was then left undisturbed. The gelation process took several hours to complete. The solution pH after NaOH addition was 9.1 ± 1.1 , the solution pH after GdL addition was 3.9 ± 1.1 [50]. The final concentration of peptide in the hydrogel was $C_{\text{Fmoc-FF}} = 0.6\%$. After the preparation of hydrogels by both methods, they were carefully washed out with PBS solution for 2 days to ensure complete removal of DMSO [22] (in the case of the solvent-switch method) and also to achieve hydrogel pH 7.3 instead of pH 4 [24]. The Fmoc-FF hydrogels in which the low molecular weight ($M = 190$ kDa) chitosan was added was prepared as follows: the peptides were dissolved in dimethyl sulfoxide (DMSO) to obtain the stock solution, $C_{\text{Fmoc-FF (stock)}} = 10\%$, chitosan was dissolved in HCl (1 M), $C_{\text{chitosan (stock)}} = 1\%$. The chitosan was added into the water to obtain the final concentration 0.6%, $C_{\text{chitosan (final)}} = 0.06\%$, after that the Fmoc-FF stock solution was mixed with it in such a way to obtain $C_{\text{Fmoc-FF (final)}} = 0.6\%$, so $C_{\text{Fmoc-FF}}:C_{\text{chitosan}}=10:1$. The hydrogel was washed out for several hours with PBS buffer to obtain the final pH of hydrogel 7.3.

Chemical structure (Fig. S7A) and Fourier Transform InfraRed (FTIR) analysis (Fig. S7B) are inserted in Fig. S7 for thorough characterization of the investigated hydrogel.

(C) Cell culturing.

MCF-7 cell lines were grown in DMEM F/12 complete culture medium (PanEco, Russia) containing 10% fetal calf serum (FBS) (Gibco, USA), 1x PenStrep (Gibco, USA) and 1x GlutaMax (Gibco, USA) in a standard culture incubator containing 5% CO₂ and maintained at 37 °C. For staining and subsequent CIPM assay, cells were seeded on gels formed on confocal cups at an amount of 300,000 per cup and incubated at 37 °C, 5% CO₂ for 24 hours. Cells seeded on confocal cups without gels were used as control.

For cytotoxicity test, cells were seeded into the wells of 96-well plates 24 h before the experiment in the amount of 12 thousand cells per well. After the incubation period eluted media was added to the wells with cells and the cells were incubated at 37 °C, 5% CO₂ for a day. As a control, wells with cells in which the medium was changed normally were taken.

4.2. Scanning ion-conductance microscopy (SICM) measurements

The SICM method (ICAPPIC Limited, UK) was employed to study the topography and mechanical properties of the hydrogel. The Olympus IX73 inverted optical microscope (Japan) was utilized in the experimental processes. The ICAPPIC Universal Controller and Piezo Control System (ICAPPIC Limited, UK) managed the feedback control and piezo positioning. A P-2000 laser puller (Sutter Instruments, USA) produced borosilicate glass pipettes for topography analysis. The exact radius of capillary R_{cap} value was determined using a formula [60]:

$$I = \pi R_{\text{cap}} k V \tan(\alpha) \quad (1)$$

Here, I signifies ion current, α denotes a half-cone angle, which was equal to 3 degrees, k is $1,35 \text{ Sm}^{-1}$, and V represents the applied voltage, which was 200 mV in the experiment. The hydrogel's topography was examined using the noncontact hopping mode, with a decrease in ion current of 0.5% and a scan size of $20 \times 20 \mu\text{m}$ or $25 \times 25 \mu\text{m}$. The final image resolution was 256×256 pixels. The fall rate during topography studies was set at $120 \mu\text{m} \cdot \text{s}^{-1}$.

For the hydrogel Young's modulus values the empirical formula was applied [41]:

$$E = pA/(S_{sub}/S_{samp} - 1) = pA/(d_{sub}/d_{samp} - 1) \quad (2)$$

where E represents Young's modulus and A signifies a constant reliant on the pipette's geometric attributes. The geometrical parameter A for different values of inner half cone angle α and wall thickness of the pipette is presented in Table S1 in [41]. The parameters of applied radii R , ion currents I and colloidal pressures can be seen in Table S1.

The pressure applied is denoted as p , while S_{sub} and S_{samp} refer to the current-distance curve slopes for a 1% and 2% decrease in ion current for a substrate and a sample, respectively. The current-distance curve slopes are defined by current drop of 1% and 2% and indentations of the substrate and the sample d_{sub} and d_{samp} . Since current drop is the same for both the substrate and the sample, to obtain the mechanics map, it is necessary to record the deformation on the substrate and the sample at a current drop of 1% and 2% and applied pressures.

In our study, we utilized equation (2) to determine the pressure p , colloidal pressure, which was derived from the DLVO theory, accounting for the inherent colloidal pressure that develops within the interfacial liquid layers as they become significantly compressed when the pipette is brought near the sample. It should be noted that usually the Debye length in PBS solution is considered as 1 nm. However, that is correct if only electrostatic interactions of double layers are considered. Clarke, et.al. clearly explained that interlayers did not only contribute to electrostatic forces at separation of the size and magnitude of the Hamaker constant across gaps of tens of nanometers because of the drastic variations in permittivity across these interlayers [61].

In the experiment the pressure p was estimated based on the intrinsic force as detailed by Kolmogorov et al. [36], where it was calculated on the example of decan drop. The derived formula for the intrinsic force F was expressed as: $F = 4\pi\sigma(R_{cap} \cdot d)^{1/2}$, where σ represents the surface tension coefficient, R – radius of capillary and d – indentation. The colloidal pressure was determined as $p = F/S = F/\pi a^2$, where a is a contact radius, $a = (R_{cap} \cdot d)^{1/2}$. A detailed explanation of the force and pressure calculations based on the experimental parameters is provided in the SI.

When assessing the mean value E for cells on hydrogels, more than 40 cells were analyzed (both for cells on Fmoc-FF hydrogel and for cells on Fmoc-FF+chitosan hydrogel). To determine this parameter with the highest accuracy, individual cells or hydrogels were separately identified in each frame, and the mean value E was calculated for these objects.

4.3. Fluorescence study of stained cells. Confocal measurements.

In order to obtain the fluorescence image of stained cell nuclei and microtubules, that consist of tubulin, the light from the light-emitting diode (LED) was focused on samples with the use of DAPI filter set 49 ($\lambda_{ex}=365 \text{ nm}$, $\lambda_{em}=445 \text{ nm}$) and GFP filter set 38HE eGFP ($\lambda_{ex}=470$, $\lambda_{em}=525 \text{ nm}$). The experimental setup can be seen in Fig. S8.

513 For the visualization of microtubules within MCF-7 cells via fluorescence studies,
514 the cells were labeled with TubulinTracker™ Green at a final concentration of 1 µg/mL.
515 Cells were incubated with the dye at 37 °C, 5% CO₂ for 1 hour in DMEM/F-12 complete
516 nutrient medium. Cells were also stained with Hoechst dye at a final concentration of 5
517 µg/ml (8.115 µM) to visualize cells nuclei. Hoechst was added to cells 20 minutes before
518 the end of incubation with Tubulin Tracker. After the end of incubation time, cells were
519 washed with HBSS 1-2 times.

520 4.4. Atomic force microscopy measurements

521 Atomic Force Microscopy (AFM) method was used for the assessment of
522 cell-hydrogel system stiffness using a Bruker Bioscope Resolve AFM (Bruker, USA). For
523 these tests, the implementation of Force Volume mode to determine mechanical attrib-
524 utes was applied. The PeakForce QNM-Live Cell probes (PFQNM-LC-A-CAL, Bruker
525 AFM Probes, Camarillo, CA, USA) with a pre-calibrated spring constant (around 0.1
526 N/m) and a parabolic tip with a radius of 70 nm (for estimation of tip shape see Fig. S9),
527 were used. Images of 80×80 µm² were obtained at a resolution ranging from 40×40 to
528 80×80 pixels. Force curves were acquired at a piezo speed of 180 µm·s⁻¹, with a force
529 set-point between 0.5-1 nN. The indentation depth varied from 500 to 1500 nm in the tests
530 depending on the stiffness of the sample.

531 Hertz's model was used for the numerical processing of force curves using the
532 MATLAB routine (The MathWorks, Natick, MA) [62]:

$$533 F(\delta) = (4R_{tip}^{1/2}/3 \cdot (1 - \nu^2))E\delta^{3/2} \quad (3)$$

534

535 In this model, F represents the force acting on the cantilever tip, δ is the indentation
536 depth, R_{tip} stands for the indenter radius, ν is the Poisson's ratio of the sample (assumed
537 to be 0,5 for the cells [63, 64] and hydrogel [65] as it was shown that they maintain their
538 volume under load), and E is the Young's modulus. The model characterizes the inden-
539 tation of a parabolic tip into an elastic half-space and is applicable to indentation depths
540 exceeding the tip radius [66]. Here the indentation range for the fit was limited to 500 nm.
541 In AFM experiments, to determine the Young's modulus, the fit was applied only to the
542 initial 500 nm of indentation depth for investigated systems. This range fell within the
543 applicability range of the Hertz model for the AFM probes with parabolic tips used, as
544 demonstrated in previous studies [66, 67] While the Hertz model can be used for spher-
545 ical indenters at depths below the sphere's radius, the parabolic tip shape does not have
546 this limitation [68]. Additionally, the tip shape was analyzed by scanning a calibration
547 grating and was well-fitted with a quadratic function up to 500 nm of tip height. The es-
548 timated radius of curvature at the peak matched well with the tip radius provided by the
549 probe manufacturer (70 nm ± 10%). The chosen depth of 500 nm allows for the analysis of
550 samples within the same surface layer, independent of local stiffness and the highest
551 applied load. Limiting the indentation depth also helps to remain within the linear elastic
552 regime of the material [69]. For the tips used, a transition from a paraboloid to a 3-sided
553 pyramid occurs after an indentation of around 550 nm [66]

554 The regions with cells and bare gel surface were selected on the force volume maps.
555 Force curves with low quality of the fit were excluded from the analysis. More than 40
556 cells and 15 bare gel areas were analyzed per sample.

557 4.5. Swelling and degradation of Fmoc-FF hydrogel

To acquire insights into the physical structure of Fmoc-FF hydrogels, we assessed the swelling ratio for samples. Swelling ratios for Fmoc-FF hydrogels with identical initial total concentrations were determined using PBS. Initially, all Fmoc peptide-based hydrogels were weighed (W_i). Subsequently, 3 ml of PBS (pH 7.4) were added to each hydrogel, which were then incubated at 37°C overnight. The fully swollen hydrogels were weighed (W_s) immediately after the removal of excess water. Following this, the hydrogels were freeze-dried and weighed again (W_d). The swelling behavior was quantified as the swelling ratio q (%), defined as the ratio of the swollen sample weight (W_s) to the freeze-dried hydrogel weight (W_d) ($q=(W_s-W_d)/W_s \cdot 100$). The mass loss was determined by the formula $\Delta W=W_s/W_i$.

4.6. MTT test

For the MTT test, gels were prepared in a 96-well plate under sterile conditions and washed 5 times with DPBS overnight. Then the gels were incubated at 37°C, 5% CO₂ with complete culture medium overnight. The eluted medium was transferred to cells in a 96-well plate. The cells were incubated with transferred medium for 24 hours, after that the MTT test was carried out: the medium with MTT reagent was added, the cells were incubated for 4 hours, then the medium with reagent was withdrawn, DMSO was added and cells were incubated on a shaker for 15 minutes. Fluorescence intensity was measured using a multi-plate reader (Varioskan LUX, Thermo Fisher Scientific, Inc.)

4.7. Live/dead test

The percentage of surviving cells on the gels was determined by staining them with two fluorescent dyes: C12 Resazurin – red dye, which stains the membrane of metabolically active cells, and DAPI - blue dye, which stains DNA in cells with damaged membrane (late apoptotic and necrotic).

Gels were prepared under sterile conditions in confocal Petri dishes, then washed 5 times with DPBS for a day. Afterward, cells were seeded on the dishes at the rate of 300,000/dish. The cells were incubated at 37°C, 5% CO₂ for 48 hours. At the end of incubation period, cells were stained: DAPI ($C_{\text{DAPI}}=1\text{mM}$) and C12 Resazurin ($C_{\text{res}}=0.5\text{mM}$) were added; incubation with dyes was carried out at 37°C, 5% CO₂ for 10 minutes. The live/dead test measurements were carried out using inverted fluorescence microscope (EVOS M5000 Imaging System, Thermo Fisher Scientific).

5. Conclusions

The aim of the article was to explore what new possibilities or information the alternative Scanning Ion-Conductance Microscopy (SICM) method can provide compared to the traditional Atomic Force Microscopy (AFM) method in studying the mechanical properties of the cell-hydrogel system. To the best of our knowledge, there are no studies that have produced maps of the mechanical property distribution of cell-hydrogel systems where the substrate is softer than the cell itself. Such systems might be of interest in the field of regenerative medicine for the restoration of soft tissues, such as soft brain tissue, $E \sim 0.1\text{-}1\text{ kPa}$ [10], or adipose tissues $E \sim 1\text{-}2\text{ kPa}$ [11]. The use of this method allowed us, firstly, to simultaneously obtain a distribution map of both the soft hydrogel and the living cell. Such measuring gives the opportunity to examine the immediate change of cell's mechanical properties in response to scaffold behavior, which is important in the field of regenerative medicine when testing the effects of different drugs on the cell-scaffold system. Secondly, the measurements carried out with SICM were in agreement with the AFM technique. One of the main advantages of SICM over AFM is its non-invasiveness; therefore, the data obtained in this study suggest that the SICM method can be used as an independent method for measuring the mechanical properties

of the cell-soft hydrogel system. Thanks to its non-destructive nature, it allows for the investigation of the dynamics of the same cell on the hydrogel over a long period, which cannot be achieved with the traditional AFM method. This capability is also important for obtaining more accurate information about changes in cell metabolism during their interaction with the scaffold. Furthermore, studies using confocal microscopy showed that the mechanical property distribution map of the cell on the hydrogel obtained by the SICM method describes specific cellular structures (nucleus/cytoskeleton), allowing for a more detailed description of changes in cell biomechanics during interaction with the hydrogel.

The biocompatibility tests demonstrated the poor cell viability on the Fmoc-FF hydrogel, though the incorporation of chitosan into self-assembled hydrogel improved the obtained value. In the future, it is planned to modify the composition of the gel to make it more suitable as a biocompatible scaffold for living cells. This could be achieved, for example, by adding other peptides such as Fmoc-F5 or PEG8-(FY)3 hexapeptide [22]. Subsequently, specific tissue types can be targeted by using epithelial or neuronal cells (depending on the task at hand). This will allow for the dynamic study of changes in cell metabolism when adhered to the surface of self-assembling gels, the effects of growth factors and other substances on the systems under investigation, and simultaneously, the degradation of the gel itself using the SICM method. The carried-out procedure can be adapted for the investigation of any cell-soft hydrogel system in order to identify the most biocompatible soft hydrogel for the application in regenerative medicine.

Supplementary Materials: The following supporting information can be downloaded at: www.mdpi.com/xxx/s1, Figure S1: Fluorescence confocal microscopy image of self-assembly Fmoc-FF hydrogel structure obtained at 405 nm excitation following staining with 10 μ M Thioflavin T; Figure S2: Profiles of MCF-7 cells placed on Petri dish (control) and Fmoc-FF hydrogel; Figure S3: The histogram of Young's modulus distribution for MCF-7 cells placed on cultural Petri dish (control, black lines), Fmoc-FF hydrogel (red lines) and Fmoc-FF+chitosan hydrogel (violet lines); Figure S4: Force curves for (A) MCF-7 on Petri dish, (B) MCF-7 on Fmoc-FF hydrogel, (C) MCF-7 on Fmoc-FF+chitosan hydrogel, (D) Fmoc-FF hydrogel, (E) Fmoc-FF+chitosan hydrogel; Figure S5: The degradation of Fmoc-FF hydrogel; Figure S6: (A) Live-dead staining of MCF-7 cells after placing them on the Fmoc-FF hydrogels for 48 h. Red staining indicates live cells, blue staining indicates dead cells. (B) MTT test of MCF-7 cells on Fmoc-FF based hydrogels; Table S1: The parameters of SICM and AFM experiments; Figure S7: (A) Chemical structures of Fmoc-FF. (B) The FTIR analysis for Fmoc-FF hydrogel; Table S1: The parameters of SICM and AFM experiments; Figure S8: Schematic representation of SICM experimental setup that allows the simultaneous topographical, quantitative nanomechanical mapping and fluorescence imaging representation; Figure S9: Estimation of the tip shape by scanning the TGT1 calibration grating. (A) Topography of TGT1 calibration grating acquired with the PFQNM-LC-A-CAL probe. (B) 3D representation of the same image. (C) Cross-section over one of the peaks fitted with a quadratic function (red curve).

Author Contributions: T.T.N. – Investigation, Analysis, Writing Original Draft; B.N.V., E.Y.M., M.-N.V.V. and K.V.S. – Investigation, Analysis; T.P.S. and S.N.N. – analysis, Review&Editing; F.V.V. - Methodology, Data Curation; G.P.V. and E.A.S. – Methodology, Review&Editing; A.-A.L. - Conceptualization, Methodology; S.E.A. - Conceptualization, Methodology, Analysis, Writing Original Draft.

Funding: The work was supported by Russian Science Foundation, grant №23-75-00007 (all experiments except AFM) and by grant No. 23-74-10113 (<https://rscf.ru/en/project/23-74-10113/>, AFM experiments and AFM data processing).

Conflicts of Interest: The authors declare no conflicts of interest.

References

- 657 1. Liu, Z.; Tang, M.; Zhao, J.; Chai, R.; Kang, J. Looking into the future: toward advanced 3D biomaterials for
658 stem-Cell-based regenerative medicine. *Adv. Mater.* **2018**, *30*, 1705388.
- 659 2. Pina, S.; Ribeiro, V.P.; Marques, C.F.; Maia, F.R.; Silva, T.H.; Reis, R.L.; Oliveira, J.M. Scaffolding strategies for tissue
660 engineering and regenerative medicine applications. *Mater.* **2019**, *12*, 1824.
- 661 3. Tang, Y.; Wang, H.; Liu, S.; Pu, L.; Hu, X.; Ding, J.; Xu, G.; Xu, W.; Xiang, S.; Yuan, Z. A review of protein hydrogels:
662 protein assembly mechanisms, properties, and biological applications. *Colloids Surf. B Biointerfaces* **2022**, *220*, 112973.
- 663 4. Liang, Y.; He, J.; Guo, B. Functional hydrogels as wound dressing to enhance wound healing. *ACS Nano* **2021**, *15*,
664 12687-12722.
- 665 5. Borro, B.C.; Nordström, R.; Malmsten, M. Microgels and hydrogels as delivery systems for antimicrobial peptides.
666 *Colloids Surf. B Biointerfaces* **2020**, *187*, 110835.
- 667 6. Lou, J.; Mooney, D.J. Chemical strategies to engineer hydrogels for cell culture. *Nat. Rev. Chem.* **2022**, *6*, 726-744.
- 668 7. Stowers, R.S. Advances in extracellular matrix-mimetic hydrogels to guide stem cell fate. *Cells Tissues Organs* **2022**,
669 *211*, 703-720.
- 670 8. Tayler, I.M.; Stowers, R.S. Engineering hydrogels for personalized disease modeling and regenerative medicine.
671 *Acta Biomater.* **2021**, *132*, 4-22.
- 672 9. Halperin-Sternfeld, M.; Pokhojaev, A.; Ghosh, M.; Rachmiel, D.; Kannan, R.; Grinberg, I.; Asher, M.; Aviv, M.; Ma,
673 P.X.; Binderman, I.; Sarig, R.; Adler-Abramovich, L. Immunomodulatory fibrous hyaluronic ac-
674 id-Fmoc-diphenylalanine-based hydrogel induces bone regeneration. *J. Clin. Periodontol.* **2023**, *50*, 200-219.
- 675 10. Wang, T.W.; Spector, M. Development of hyaluronic acid-based scaffolds for brain tissue engineering. *Acta Bio-*
676 *mater.* **2009**, *5*, 2371-2384.
- 677 11. Van Nieuwenhove, I.; Tytgat, L.; Ryx, M.; Blondeel, P.; Stillaert, F.; Thienpont, H.; Ottevaere, H.; Van Vlierberghe,
678 S. Soft tissue fillers for adipose tissue regeneration: from hydrogel development toward clinical applications. *Acta Bi-*
679 *omater.* **2017**, *63*, 37-49.
- 680 12. Xu, Y.; Patnaik, S.; Guo, X.; Li, Z.; Lo, W.; Butler, R.; Claude, A.; Liu, Z.; Zhang, G.; Liao, J.; Anderson, P.M.; Guan, J.
681 Cardiac differentiation of cardiosphere-derived cells in scaffolds mimicking morphology of the cardiac extracellular
682 matrix. *Acta Biomater.* **2014**, *10*, 3449-3462.
- 683 13. Zhang, X.; Li, X.W.; Li, J.G.; Sun, X.D. Preparation and mechanical property of a novel 3D porous magnesium
684 scaffold for bone tissue engineering. *Mater. Sci. Eng.: C* **2014**, *42*, 362-367.
- 685 14. Hu, Q.; Liu, M.; Chen, G.; Xu, Z.; Lv, Y. Demineralized bone scaffolds with tunable matrix stiffness for efficient
686 bone integration. *ACS Appl. Mater. Interfaces* **2018**, *10*, 27669-27680.
- 687 15. Gyles, D.A.; Castro, L.D.; Silva, J.O.C., Jr.; Ribeiro-Costa, R.M. A review of the designs and prominent biomedical
688 advances of natural and synthetic hydrogel formulations. *Eur. Polym. J.* **2017**, *88*, 373-392.
- 689 16. Tibbitt, M.W.; Anseth, K.S. Hydrogels as extracellular matrix mimics for 3D cell culture. *Biotechnol. Bioeng.* **2009**,
690 *103*(4), 655-663.
- 691 17. Sun, B. The mechanics of fibrillar collagen extracellular matrix. *Cell Rep. Phys. Sci.* **2021**, *2*(8).
- 692 18. Gilarska, A.; Lewandowska-Łańcucka, J.; Horak, W.; Nowakowska, M. Collagen/chitosan/hyaluronic acid-based
693 injectable hydrogels for tissue engineering applications—design, physicochemical and biological characterization. *Col-*
694 *loids Surf. B Biointerfaces* **2018**, *170*, 152-162.
- 695 19. Halper, J.; Kjaer, M. Basic components of connective tissues and extracellular matrix: elastin, fibrillin, fibulins, fi-
696 brinogen, fibronectin, laminin, tenascins and thrombospondins. *Prog. Heritable Soft Connect. Tissue Dis.* **2014**, 31-47.
- 697 20. Nelson, D.W.; Gilbert, R.J. Extracellular matrix-mimetic hydrogels for treating neural tissue injury: a focus on fi-
698 brin, hyaluronic acid, and elastin-like polypeptide hydrogels. *Adv. Healthc. Mater.* **2021**, *10*(22), 2101329.

- 699 21. Basavalingappa, V.; Guterman, T.; Tang, Y.; Nir, S.; Lei, J.; Chakraborty, P.; Schnaider, L.; Reches, M.; Wei, G.;
700 Gazit, E. Expanding the functional scope of the fmoc-diphenylalanine hydrogelator by introducing a rigidifying and
701 chemically active urea backbone modification. *Adv. Sci.* **2019**, *6*(12), 1900218.
- 702 22. Diaferia, C.; Ghosh, M.; Sibillano, T.; Gallo, E.; Stornaiuolo, M.; Giannini, C.; Morelli, G.; Adler-Abramovich, L.;
703 Accardo, A. Fmoc-FF and hexapeptide-based multicomponent hydrogels as scaffold materials. *Soft Matter* **2019**, *15*(3),
704 487-496.
- 705 23. Vitale, M.; Ligorio, C.; McAvan, B.; Hodson, N.W.; Allan, C.; Richardson, S.M.; Hoyland, J.A.; Bella, J. Hydroxyap-
706 atite-decorated Fmoc-hydrogel as a bone-mimicking substrate for osteoclast differentiation and culture. *Acta Biomater.*
707 **2022**, *138*, 144-154.
- 708 24. Tikhonova, T.N.; Kolmogorov, V.S.; Timoshenko, R.V.; Vaneev, A.N.; Cohen-Gerassi, D.; Osminkina, L.A.; Gorel-
709 kin, P.V.; Erofeev, A.S.; Sysoev, N.N.; Adler-Abramovich, L.; Shirshin, E.A. Sensing cells-peptide hydrogel interaction
710 in situ via scanning ion conductance microscopy. *Cells* **2022**, *11*, 4137.
- 711 25. Tikhonova, T.N.; Cohen-Gerassi, D.; Arnon, Z.A.; Efremov, Y.; Timashev, P.; Adler-Abramovich, L.; Shirshin, E.A.
712 Tunable self-assembled peptide hydrogel sensor for pharma cold supply chain. *ACS Appl. Mater. Interfaces* **2022**, *14*(50),
713 55392-55401.
- 714 26. Ramaswamy, Y.; Roohani, I.; No, Y.J.; Madafiglio, G.; Chang, F.; Zhao, F.; Zreiqat, H. Nature-inspired topogra-
715 phies on hydroxyapatite surfaces regulate stem cells behaviour. *Bioact. Mater.* **2021**, *6*(4), 1107-1117.
- 716 27. Farzarian, K.; Ghahremaninezhad, A. On the effect of chemical composition on the desorption of superabsorbent
717 hydrogels in contact with a porous cementitious material. *Gels* **2018**, *4*(3), 70.
- 718 28. Yu, S.; Liu, D.; Wang, T.; Lee, Y.Z.; Wong, J.C.N.; Song, X. Micropatterning of polymer substrates for cell culture.
719 *J. Biomed. Mater. Res. B Appl. Biomater.* **2021**, *109*(10), 1525-1533.
- 720 29. Wang, T.; Lai, J.H.; Yang, F. Effects of hydrogel stiffness and extracellular compositions on modulating cartilage
721 regeneration by mixed populations of stem cells and chondrocytes in vivo. *Tissue Eng. Part A* **2016**, *22*(23-24),
722 1348-1356.
- 723 30. Lomboni, D.J.; Steeves, A.; Schock, S.; Bonetti, L.; De Nardo, L.; Variola, F. Compounded topographical and phys-
724 icochemical cueing by micro-engineered chitosan substrates on rat dorsal root ganglion neurons and human mesen-
725 chymal stem cells. *Soft Matter* **2021**, *17*(21), 5284-5302.
- 726 31. Trkov, S.; Eng, G.; Di Liddo, R.; Parnigotto, P.P.; Vunjak-Novakovic, G. Micropatterned three-dimensional hydro-
727 gel system to study human endothelial-mesenchymal stem cell interactions. *J. Tissue Eng. Regen. Med.* **2010**, *4*(3),
728 205-215.
- 729 32. Xue, B.; Tang, D.; Wu, X.; Xu, Z.; Gu, J.; Han, Y.; Zhu, Z.; Qin, M.; Zou, X.; Wang, W.; Cao, Y. Engineering hydro-
730 gels with homogeneous mechanical properties for controlling stem cell lineage specification. *Proc. Natl. Acad. Sci.* **2021**,
731 *118*(37), e2110961118.
- 732 33. Cha, C.; Soman, P.; Zhu, W.; Nikkhah, M.; Camci-Unal, G.; Chen, S.; Khademhosseini, A. Structural reinforcement
733 of cell-laden hydrogels with microfabricated three dimensional scaffolds. *Biomater. Sci.* **2014**, *2*(5), 703-709.
- 734 34. Witkowska-Zimny, M.; Walenko, K.; Wrobel, E.; Mrowka, P.; Mikulska, A.; Przybylski, J. Effect of substrate stiff-
735 ness on the osteogenic differentiation of bone marrow stem cells and bone-derived cells. *Cell Biol. Int.* **2013**, *37*(6),
736 608-616.
- 737 35. Chen, L.; Wu, C.; Wei, D.; Chen, S.; Xiao, Z.; Zhu, H.; Luo, H.; Sun, J.; Fan, H. Biomimetic mineralized microenvi-
738 ronment stiffness regulated BMSCs osteogenic differentiation through cytoskeleton mediated mechanical signaling
739 transduction. *Mater. Sci. Eng. C* **2021**, *119*, 111613.

- 740 36. Magazzù, A.; Marcuello, C. Investigation of soft matter nanomechanics by atomic force microscopy and optical
741 tweezers: A comprehensive review. *Nanomaterials* **2023**, *13*, 963.
- 742 37. Dao, M.; Lim, C.T.; Suresh, S. Mechanics of the human red blood cell deformed by optical tweezers. *J. Mech. Phys.*
743 *Solids* **2003**, *51*, 2259–2280.
- 744 38. Agrawal, R.; Smart, T.; Nobre-Cardoso, J.; Richards, C.; Bhatnagar, R.; Tufail, A.; Shima, D.; Jones, P.H.; Pavesio, C.
745 Assessment of red blood cell deformability in type 2 diabetes mellitus and diabetic retinopathy by dual optical twee-
746 zers stretching technique. *Sci. Rep.* **2016**, *6*, 15873.
- 747 39. Kim, S.H.; et al. Magnetic Resonance Elastography for the Detection and Classification of Prostate Cancer. *Cancers*
748 **2024**, *16*, 3494.
- 749 40. Kolmogorov, V.S.; Erofeev, A.S.; Woodcock, E.; Efremov, Y.M.; Iakovlev, A.P.; Savin, N.A.; Alova, A.V.; Lavrush-
750 kina, S.V.; Kireev, I.I.; Prelovskaya, A.O.; Sviderskaya, E.V.; Scaini, D.; Klyachko, N.L.; Timashev, P.S.; Takahashi, Y.;
751 Salikhov, S.V.; Parkhomenko, Y.N.; Majouga, A.G.; Edwards, C.R.W.; Novak, P.; Korchev, Y.E.; Gorelkin, P.V. Map-
752 ping mechanical properties of living cells at nanoscale using intrinsic nanopipette–sample force interactions. *Nanoscale*
753 **2021**, *13*(13), 6558–6568.
- 754 41. Rheinlaender, J.; Schäffer, T.E. Mapping the mechanical stiffness of live cells with the scanning ion conductance
755 microscope. *Soft Matter* **2013**, *9*(12), 3230–3236.
- 756 42. Seifert, J.; Rheinlaender, J.; von Eysmond, H.; Schäffer, T.E. Mechanics of migrating platelets investigated with
757 scanning ion conductance microscopy. *Nanoscale* **2022**, *14*(22), 8192–8199.
- 758 43. Franchi, M.; Masola, V.; Karamanos, K.A.; Franchi, L.; Kyriakopoulou, K.; Onisto, M.; Cappadone, C. Basement
759 Membrane, Collagen, and Fibronectin: Physical Interactions with Cancer Cells. In *The Extracellular Matrix and the*
760 *Tumor Microenvironment*; Springer International Publishing: Cham, 2022; pp. 247–277.
- 761 44. Gaeta, I.M.; Meenderink, L.M.; Postema, M.M.; Cencer, C.S.; Tyska, M.J. Direct visualization of epithelial microvilli
762 biogenesis. *Curr. Biol.* **2021**, *31*, 2561–2575.
- 763 45. Boido, M.; Ghibaudi, M.; Gentile, P.; Favaro, E.; Fusaro, R.; Tonda-Turo, C. Chitosan-based hydrogel to support the
764 paracrine activity of mesenchymal stem cells in spinal cord injury treatment. *Sci. Rep.* **2019**, *9*, 6402.
- 765 46. Demirtaş, T.T.; Irmak, G.; Gümüşderelioğlu, M. A bioprintable form of chitosan hydrogel for bone tissue engi-
766 neering. *Biofabrication* **2017**, *9*, 035003.
- 767 47. Ji, C.; Khademhosseini, A.; Dehghani, F. Enhancing cell penetration and proliferation in chitosan hydrogels for
768 tissue engineering applications. *Biomater.* **2011**, *32*, 9719–9729.
- 769 48. Ferreira, D.P.; Conceição, D.S.; Calhella, R.C.; Sousa, T.; Socoteanu, R.; Ferreira, I.C.; Ferreira, L.V. Porphyrin dye
770 into biopolymeric chitosan films for localized photodynamic therapy of cancer. *Carbohydr. Polym.* **2016**, *151*, 160–171.
- 771 49. He, K.; Wang, X. Rapid prototyping of tubular polyurethane and cell/hydrogel constructs. *J. Bioact. Compat. Polym.*
772 **2011**, *26*, 363–374.
- 773 50. Adams, D.J.; Mullen, L.M.; Berta, M.; Chen, L.; Frith, W.J. Relationship between molecular structure, gelation be-
774 haviour and gel properties of Fmoc-dipeptides. *Soft Matter* **2010**, *6*(9), 1971–1980.
- 775 51. Taira, N.; Nashimoto, Y.; Ino, K.; Ida, H.; Imaizumi, T.; Kumatani, A.; Takahashi, Y.; Shiku, H. Micropipet-based
776 navigation in a microvascular model for imaging endothelial cell topography using scanning ion conductance mi-
777 croscopy. *Anal. Chem.* **2021**, *93*, 4902–4908.
- 778 52. Schierbaum, N.; Rheinlaender, J.; Schäffer, T.E. Combined atomic force microscopy (AFM) and traction force mi-
779 croscopy (TFM) reveals a correlation between viscoelastic material properties and contractile prestress of living cells.
780 *Soft Matter* **2019**, *15*, 1721–1729.

- 781 53. Rheinlaender, J.; Dimitracopoulos, A.; Wallmeyer, B.; Kronenberg, N.M.; Chalut, K.J.; Gather, M.C.; Betz, T.; Char-
782 rras, G.; Franze, K. Cortical cell stiffness is independent of substrate mechanics. *Nat. Mater.* **2020**, *19*, 1019-1025.
- 783 54. Hoglebe, N.J.; Gooch, K.J. Direct influence of culture dimensionality on human mesenchymal stem cell differentia-
784 tion at various matrix stiffnesses using a fibrous self-assembling peptide hydrogel. *J. Biomed. Mater. Res. A* **2016**, *104*,
785 2356-2368.
- 786 55. Vernerey, F.J.; Sridhar, S.L.; Muralidharan, A.; Bryant, S.J. Mechanics of 3D cell–hydrogel interactions: Experi-
787 ments, models, and mechanisms. *Chem. Rev.* **2021**, *121*, 11085-11148.
- 788 56. Kloxin, A.M.; Kloxin, C.J.; Bowman, C.N.; Anseth, K.S. Mechanical properties of cellularly responsive hydrogels
789 and their experimental determination. *Adv. Mater.* **2010**, *22*, 3484-3493.
- 790 57. Gil-Redondo, J.C.; Weber, A.; Zbiral, B.; Toca-Herrera, J.L. Substrate stiffness modulates the viscoelastic properties
791 of MCF-7 cells. *J. Mech. Behav. Biomed. Mater.* **2022**, *125*, 104979.
- 792 58. Darnell, M.C.; Sun, J.Y.; Mehta, M.; Johnson, C.; Arany, P.R.; Suo, Z.; Mooney, D.J. Performance and biocompati-
793 bility of extremely tough alginate/polyacrylamide hydrogels. *Biomaterials* **2013**, *34*, 8042-8048.
- 794 59. Raeburn, J.; Pont, G.; Chen, L.; Cesbron, Y.; Lévy, R.; Adams, D.J. Fmoc-diphenylalanine hydrogels: understanding
795 the variability in reported mechanical properties. *Soft Matter* **2012**, *8*(4), 1168-1174.
- 796 60. Chowdhury, T.K. Fabrication of extremely fine glass micropipette electrodes. *J. Phys. E: Sci. Instrum.* **1969**, *2*(12),
797 1087.
- 798 61. Clarke, R. W.; Zhukov, A.; Richards, O.; Johnson, N.; Ostanin, V.; Klenerman, D. Pipette–surface interaction: cur-
799 rent enhancement and intrinsic force. *JACS* **2013**, *135*(1), 322-329.
- 800 62. Efremov, Y.M.; Wang, W.H.; Hardy, S.D.; Geahlen, R.L.; Raman, A. Measuring nanoscale viscoelastic parameters
801 of cells directly from AFM force-displacement curves. *Sci. Rep.* **2017**, *7*(1), 1541.
- 802 63. Efremov, Y.M.; Velay-Lizancos, M.; Weaver, C.J.; Athamneh, A.I.; Zavattieri, P.D.; Suter, D.M.; Raman, A. Anisot-
803 ropy vs isotropy in living cell indentation with AFM. *Sci. Rep.* **2019**, *9*, 5757.
- 804 64. Harris, A.R.; Charras, G.T. Experimental validation of atomic force microscopy-based cell elasticity measurements.
805 *Nanotechnology* **2011**, *22*, 345102.
- 806 65. Ahearne, M.; Yang, Y.; El Haj, A.J.; Then, K.Y.; Liu, K.K. Characterizing the viscoelastic properties of thin hydro-
807 gel-based constructs for tissue engineering applications. *J. R. Soc. Interface* **2005**, *2*, 455-463.
- 808 66. Kulkarni, S.G.; Pérez-Domínguez, S.; Radmacher, M. Influence of cantilever tip geometry and contact model on
809 AFM elasticity measurement of cells. *J. Mol. Recognit.* **2023**, *36*, e3018.
- 810 67. Efremov, Y.M.; Shpichka, A.I.; Kotova, S.L.; Timashev, P.S. Viscoelastic mapping of cells based on fast force vol-
811 ume and PeakForce Tapping. *Soft Matter* **2019**, *15*, 5455-5463.
- 812 68. Sneddon, I.N. The relation between load and penetration in the axisymmetric Boussinesq problem for a punch of
813 arbitrary profile. *Int. J. Eng. Sci.* **1965**, *3*, 47-57.
- 814 69. Rico, F.; Roca-Cusachs, P.; Gavara, N.; Farré, R.; Rotger, M.; Navajas, D. Probing mechanical properties of living
815 cells by atomic force microscopy with blunted pyramidal cantilever tips. *Phys. Rev. E* **2005**, *72*, 021914.